

Magnetic order in GdBiPt studied by x-ray resonant magnetic scattering

A. Kreyssig¹, M. G. Kim¹, J. W. Kim², S. M. Sauerbrei¹, S. D. March¹,
G. R. Tesdall¹, S. L. Bud'ko¹, P. C. Canfield¹, R. J. McQueeney¹, and A. I. Goldman¹

¹Ames Laboratory, U. S. DOE and Department of Physics and Astronomy, Iowa State University, Ames, Iowa 50011, USA and

²Advanced Photon Source, Argonne National Laboratory, Argonne, Illinois 60439, USA

(Dated: February 18, 2022)

Rare earth (*R*) half-Heusler compounds, *R*BiPt, exhibit a wide spectrum of novel ground states. Recently, GdBiPt has been proposed as a potential antiferromagnetic topological insulator (AFTI). We have employed x-ray resonant magnetic scattering to elucidate the microscopic details of the magnetic structure in GdBiPt below $T_N = 8.5$ K. Experiments at the Gd L_2 absorption edge show that the Gd moments order in an antiferromagnetic stacking along the cubic diagonal $[1\ 1\ 1]$ direction satisfying the requirement for an AFTI, where both time-reversal symmetry and lattice translational symmetry are broken, but their product is conserved.

PACS numbers: 75.25.-j, 75.50.Ee, 73.20.-r

The discovery of three-dimensional topological-insulating states in binary alloys $(\text{Bi}_{1-x}\text{Sb}_x)^{1,2}$ and compounds $(\text{Bi}_2\text{Se}_3, \text{Bi}_2\text{Te}_3, \text{Sb}_2\text{Te}_3)^{3-5}$ which feature an insulating gap in the bulk but with topologically protected conducting states on the surfaces or edges, has opened a new frontier for fundamental condensed matter physics research.⁶ As pointed out in several papers, the novel properties of this class of materials offer potential for technological breakthroughs in quantum computing and magneto-electronic applications.⁶⁻⁸ Over the past year, attention has turned towards investigations of new phenomena that arise when topological insulators (TI) also manifest, or are in close proximity to, other phenomena including magnetic order and superconductivity.^{6,8-10} Recently, the Heusler and half-Heusler compounds have been subject to intense scrutiny because of their potential as TI with tunable electronic properties.¹¹⁻¹⁴ Specifically, Mong *et al.*¹⁰ have proposed that GdBiPt may provide the first realization of an antiferromagnetic topological insulator (AFTI), where both time-reversal symmetry and lattice translational symmetry are broken, but their product is conserved. Predictions for this class of TI include gapped states on some surfaces, gapless states on others, and novel one-dimensional metallic states along step edges on the gapped surfaces.¹⁰

More generally, Heusler and half-Heusler compounds exhibit a wide spectrum of novel ground states.¹⁵ The rare earth (*R*) half-Heusler compounds, *R*BiPt, feature magnetic ordering (GdBiPt),¹⁶ superconductivity (LaBiPt, YBiPt)^{17,18} and heavy-fermion behavior (YbBiPt)¹⁹. Although the low-temperature ground states of the *R*BiPt system (for *R* = Ce, Nd, Sm, Gd, Tb, Dy, Ho, Er, Tm, and Yb) have been characterized as antiferromagnetic through thermodynamic and transport measurements, there have been few magnetic structure determinations for this series.²⁰ GdBiPt has the highest T_N of the series at approximately 8.5 K¹⁶ and, since the orbital angular momentum $L = 0$ for the *S*-state Gd ion, the magnetic structure in the absence of crystalline electric field effects may be directly investigated. However, the high neutron-absorption cross section for naturally occurring Gd is problematic for conventional magnetic diffraction experiments.

Here we describe the magnetic order of GdBiPt below $T_N = 8.5$ K determined by x-ray resonant magnetic scattering (XRMS) at the Gd L_2 absorption edge. GdBiPt crystallizes

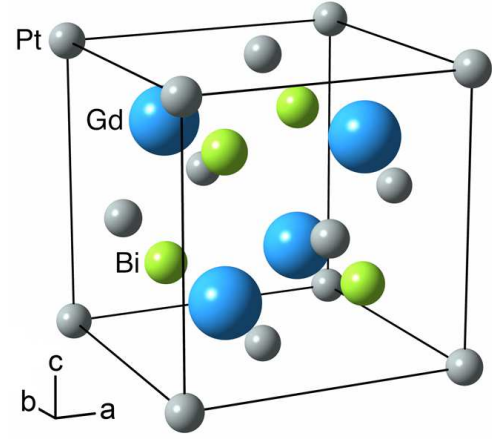


FIG. 1: (Color online) Crystal structure of GdBiPt.

in the MgAgAs-type structure (cubic space group $F\bar{4}3m$, $a = 6.68$ Å with Gd, Bi and Pt at the $4c$, $4d$ and $4a$ sites, respectively; see Fig. 1).^{21,22} The structure may be viewed as three sets of elementally pure, interpenetrating face-centered cubic lattices. We find that the commensurate magnetic order doubles the cubic unit cell along the diagonal $[1\ 1\ 1]$ direction, characterized by a propagation vector $\mathbf{q}_m = (\frac{1}{2}\ \frac{1}{2}\ \frac{1}{2})$, so that alternating ferromagnetic $(1\ 1\ 1)$ planes of Gd are antiferromagnetically coupled along the $[1\ 1\ 1]$ direction. This structure is quite similar to the model B magnetic structure for an AFTI via spin-orbit coupling as described by Mong *et al.*,¹⁰ but we find that the moment direction in GdBiPt is not parallel to the magnetic propagation vector as is found, for example, in MnSbCu²³ or CeBiPt.²⁰

Single crystals of GdBiPt were solution-grown using a Bi flux and emerged with sizeable facets perpendicular to the $[001]$ direction and smaller facets perpendicular to $[1\ 1\ 1]$. High-purity Gd (obtained from Ames Laboratory), Pt, and Bi were placed in an alumina crucible in the ratio Gd:Pt:Bi = 3:3:94, sealed in a silica ampule, and slowly cooled from 1170°C to 600°C over 200 hours. At 600°C, the excess Bi solution was decanted from the GdBiPt crystals.²⁴ The dimensions of the single crystal studied in the XRMS

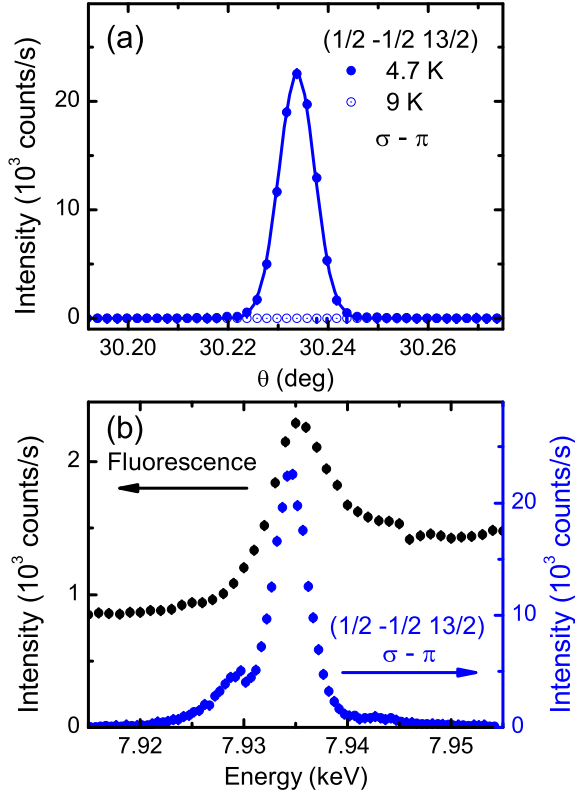


FIG. 2: (Color online) Resonant magnetic scattering from the GdBiPt single crystal. (a) Rocking scans (θ) through the $(\frac{1}{2} - \frac{1}{2} \frac{13}{2})$ magnetic peak position above (open circles) and below (filled circles) T_N taken in σ - π scattering geometry. (b) Energy scan through the Gd L_2 absorption edge at the $(\frac{1}{2} - \frac{1}{2} \frac{13}{2})$ magnetic peak position at $T = 4.7$ K (blue filled circles) along with the measured x-ray fluorescence from the sample (black filled circles).

measurements were approximately $3 \times 3 \times 2$ mm³ with a large as-grown facet perpendicular to $[001]$. The measured mosaicity of the crystal was less than 0.01 degrees full-width-at-half-maximum (FWHM), attesting to the high quality of the sample. The XRMS experiment was performed on the 6ID-B beamline at the Advanced Photon Source at the Gd L_2 -edge ($E = 7.934$ keV). The incident radiation was linearly polarized perpendicular to the vertical scattering plane (σ -polarized) with a beam size of 0.5 mm (horizontal) \times 0.2 mm (vertical). In this configuration, dipole resonant magnetic scattering rotates the plane of linear polarization into the scattering plane (π -polarization). For some of the measurements, pyrolytic graphite PG (006) was used as a polarization analyzer to suppress the charge and fluorescence background relative to the magnetic scattering signal. For measurements of the magnetic reflections, the sample was mounted at the end of the cold finger of a closed-cycle cryogenic refrigerator with the (HHL) plane coincident with the scattering plane.

Measurements of the diffraction from the sample performed in the σ - π scattering geometry using the PG (006) polarization analyzer are shown in Fig. 2. For temperatures above $T_N = 8.5$ K, only Bragg peaks consistent with the chemical structure^{21,22} of GdBiPt were observed. However, upon cool-

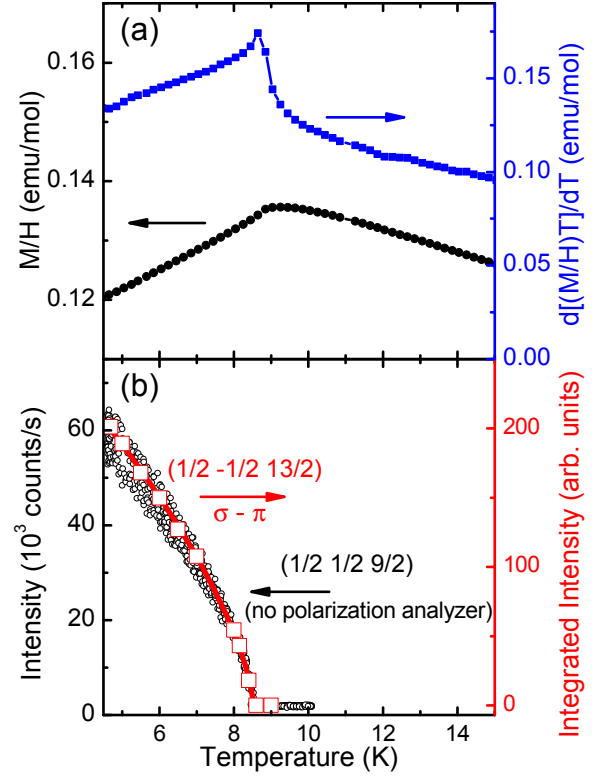


FIG. 3: (Color online) (a) M/H and its temperature derivative for GdBiPt. (b) The magnetic intensity measured while scanning temperature at the maximum of the $(\frac{1}{2} \frac{1}{2} \frac{9}{2})$ diffraction peak without a polarization analyzer (open small circles) and the integrated intensity of the $(\frac{1}{2} - \frac{1}{2} \frac{13}{2})$ diffraction peak measured at selected temperatures using the polarization analyzer (open large squares). The solid line is a power law fit to the integrated intensity data as described in the text.

ing below T_N , additional Bragg scattering at half-integer values of (HKL) was found as shown in Fig. 2(a). The magnetic origin of these peaks was confirmed by energy scans through the Gd L_2 absorption edge and from the temperature dependence of the diffraction peak intensity as described below.

The energy scan Fig. 2(b) was performed with the diffractometer set at the magnetic peak position and is typical of resonant magnetic scattering at the L edges of rare-earth compounds.²⁵ At the L_2 edge of rare-earth elements, the resonance primarily involves electric dipole ($E1$) transitions from the $2p_{\frac{1}{2}}$ core level to the empty $5d$ states, seen as the strong line just at, or slightly below the maximum in the measured fluorescence intensity. The weaker feature below the $E1$ resonance in Fig. 2(b) is likely due to the electric quadrupole ($E2$) transition from the $2p_{\frac{1}{2}}$ core level to the $4f$ states that are pulled below the Fermi energy because of the presence of the core hole in the resonance process.

The temperature dependence of the magnetic scattering, along with the corresponding magnetization measurements performed on a sample from the same batch using a Quantum Design Magnetic Properties Measurement System, are shown in Fig. 3. The magnetic order parameter was measured at the

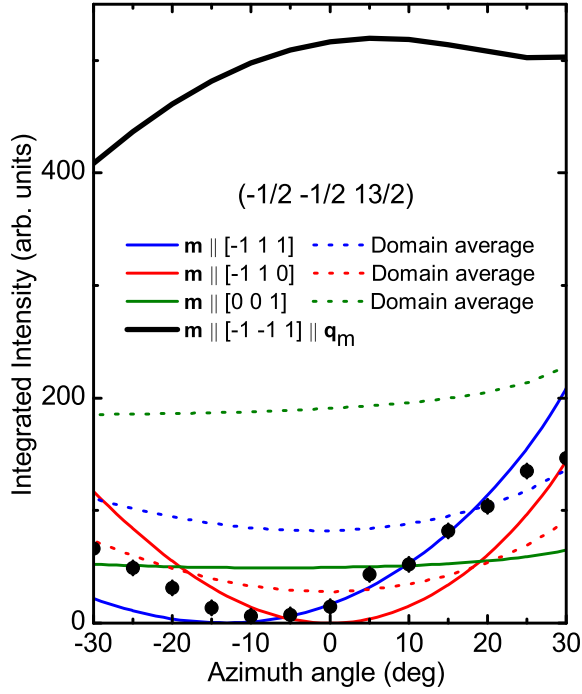


FIG. 4: (Color online) Integrated intensity in azimuth scans through the $(-\frac{1}{2} -\frac{1}{2} \frac{13}{2})$ magnetic Bragg peak. Measured data are depicted by full black circles. Full and dashed lines represent calculations for selected magnetic moment directions in a single magnetic domain, and for intensity from equally populated domains averaged over the three possible symmetry-equivalent magnetic moment orientations, respectively.

$(\frac{1}{2} \frac{1}{2} \frac{9}{2})$ peak position as the sample temperature was increased during a temperature scan in the absence of the polarization analyzer. These data were supplemented by measurements of the integrated intensity of the $(\frac{1}{2} -\frac{1}{2} \frac{13}{2})$ magnetic Bragg peak at selected temperatures and with polarization analysis. The line in Fig. 3(b) describes a fit to the integrated intensity data using a power law of the form $I \sim (1 - \frac{T}{T_N})^{2\beta}$ yielding $T_N = 8.52 \pm 0.05$ K and $\beta = 0.33 \pm 0.02$. The close proximity of T_N determined from our scattering measurements and the peak in $d[(M/H)T]/dT$ (Ref. 26) at $T = 8.6$ K, again confirms the magnetic origin of the Bragg scattering with a propagation vector of $\mathbf{q}_m = (\frac{1}{2} \frac{1}{2} \frac{1}{2})$. Systematic M versus H measurements (not shown) demonstrate in addition that no spontaneous ferromagnetic moment is present.

Having established the nature of the magnetic ordering in GdBiPt, we now describe our attempt to determine the direction of the ordered magnetic moment. The angular dependence of the resonant magnetic intensity $I(\psi)$ for the incident σ -polarized beam depends upon the component of the magnetic moment along the scattered beam direction and can be written as $I(\psi)_{(\mathbf{Q}, \alpha, \beta)} = C [\hat{\mathbf{m}} \cdot \hat{\mathbf{k}}'(\psi)_{(\mathbf{Q})}]^2 A(\psi)_{(\mathbf{Q}, \alpha, \beta)}$ where C is an overall scale factor that accounts for the resonant scattering matrix element and incident beam intensity, $\hat{\mathbf{m}}$ and $\hat{\mathbf{k}}'$ represent the magnetic moment and scattered beam directions, respectively, and A accounts for the absorption correction.²⁷ The sample geometry required off-specular scat-

tering measurements of the magnetic peaks. That is, the angle α of the incident beam \mathbf{k} with respect to the sample surface is different from the angle β of the outgoing beam \mathbf{k}' with respect to the sample surface.²⁸ For the azimuth angle ψ scans shown in Fig. 4, the diffractometer was set at the position of the magnetic Bragg peak and the crystal was rotated around the scattering vector $\mathbf{Q} = \mathbf{k}' - \mathbf{k}$ thereby rotating $\hat{\mathbf{k}}'$ with respect to $\hat{\mathbf{m}}$ while leaving \mathbf{Q} fixed. This yields an azimuth dependence of the intensity which is specific to a given magnetic moment direction. Note, that the absorption correction A also depends on the azimuth angle ψ .

For a cubic lattice, the determination of the ordered moment direction is significantly complicated by the presence of domains that arise from symmetry-equivalent magnetic propagation vectors and moment directions. For the observed magnetic Bragg peaks at $(H K L)$ with H, K , and L half integers, four symmetry-equivalent $\{\frac{1}{2} \frac{1}{2} \frac{1}{2}\}$ propagation vectors exist: $(\frac{1}{2} \frac{1}{2} \frac{1}{2})$, $(-\frac{1}{2} -\frac{1}{2} \frac{1}{2})$, $(\frac{1}{2} -\frac{1}{2} -\frac{1}{2})$, and $(-\frac{1}{2} \frac{1}{2} -\frac{1}{2})$. Fortunately, for GdBiPt in the cubic space group $F\bar{4}3m$, only one propagation vector contributes to a particular magnetic reflection [e.g. the magnetic Bragg peak $(-\frac{1}{2} -\frac{1}{2} \frac{13}{2})$ is generated by the propagation vector $\mathbf{q}_m = (-\frac{1}{2} -\frac{1}{2} \frac{1}{2})$ from the (006) zone center]. The measured data for the $(-\frac{1}{2} -\frac{1}{2} \frac{13}{2})$ magnetic Bragg peak show two important features in the azimuth scan presented in Fig. 4: a distinct minimum with almost no intensity close to $\psi = 0$, and an increase in intensity by more than an order of magnitude as ψ is varied by $\pm 30^\circ$. Both features are in strong contrast to the expected ψ dependence of the intensity for magnetic moments parallel to the propagation vector $\mathbf{q}_m = (-\frac{1}{2} -\frac{1}{2} \frac{1}{2})$ as illustrated in Fig. 4 by the bold black line with a maximum close to $\psi = 0$. Therefore, we can exclude that the moments are parallel to the propagation vector in GdBiPt.

In Fig. 4, calculated curves are also shown for other moment directions. Unfortunately, for each of the depicted moment directions, three different symmetry-equivalent orientations can occur yielding three magnetic domains. The dashed lines in Fig. 4 represent the calculated ψ dependence of the intensity if we include all such domains for a given moment direction with equal population. We again find poor agreement between the domain-averaged calculations for moments along the set of $\{1 1 1\}$, $\{1 1 0\}$ and $\{0 0 1\}$ directions. However, calculations assuming the presence of only a single domain within the probed volume, with one specified moment direction (either $[-1 1 1]$ or $[-1 1 0]$ for the $(-\frac{1}{2} -\frac{1}{2} \frac{13}{2})$ Bragg peak in Fig. 4) come much closer to describing the measured data. This behavior clearly indicates that the magnetic domains are large; smaller than the footprint of the incident beam on the sample (approximately 0.5×0.5 mm²), but of the same order of magnitude. Similar large magnetic domains have been noted in previous X RMS work on GdNi₂Ge₂ as well.²⁹ Nevertheless, a unique determination of the moment direction is not possible based on the available data. A more precise determination of the moment direction may be possible from measurements with much smaller incident beam dimensions and/or control of domain populations.²⁹

Summarising the experimental results, below $T_N = 8.5$ K

the magnetic Gd moments order in a commensurate antiferromagnetic structure in GdBiPt that can be described as doubling the cubic unit cell along the diagonal $[1\ 1\ 1]$ direction, so that alternating ferromagnetic $(1\ 1\ 1)$ planes of Gd are antiferromagnetically coupled along the $[1\ 1\ 1]$ direction. The moments are not aligned parallel to this diagonal $[1\ 1\ 1]$ direction.

In contrast to GdBiPt, CeBiPt is an antiferromagnet characterized by a propagation vector $\mathbf{q}_m = (1\ 0\ 0)$ and the ordered moments are collinear with the propagation vector along $[1\ 0\ 0]$,²⁰ but with a reduced moment that may, in part, be attributed to crystalline electric field (CEF) effects.³⁰ Unfortunately, XRMS measurements do not allow a direct extraction of the ordered moment in GdBiPt, but earlier specific heat measurements¹⁶ estimated an entropy of $\sim 0.8\mathcal{R}\ln 8$ associated with the magnetic transition close to the value expected for full moment ordering without CEF effects. The entropy associated with the corresponding magnetic transitions for the Nd, Tb and Dy compounds were considerably less than $\mathcal{R}\ln(2J+1)$ expected for the full Hund's rule J multiplet, indicating the importance of CEF effects in these compounds. The magnetic structures for $R = \text{Nd, Sm, Tb, Dy, Ho, Er, Tm, and Yb}$, have not yet been identified by neutron or XRMS measurements and such measurements are planned.

Finally, we comment on our results in light of the proposal

that GdBiPt may be an AFTI candidate.¹⁰ The AFTI state may be derived from either magnetic ordering in a pre-existing strong TI (model A in Ref. 10) or, alternatively, for specific antiferromagnetic ordering schemes that induce spin-orbit coupling in the system (model B in Ref. 10). Given previous ARPES measurements³¹ above T_N , which do not find direct evidence for band inversion in GdBiPt, it seems unlikely that GdBiPt is itself a strong TI. However, the magnetic structure determined here is consistent with the alternative model B presented by Mong *et al.*¹⁰ The doubling along the cubic diagonal direction represents the broken lattice translational symmetry (by order of two) and the ordering of each magnetic moment breaks the time-reversal symmetry, however, the product of both symmetry operations is conserved for the determined magnetic order.

We acknowledge valuable discussions with A. Kaminski, J. E. Moore, R. S. K. Mong, P. J. Ryan, and J. C. Lang. This work was supported by the Division of Materials Sciences and Engineering, Office of Basic Energy Sciences, U. S. Department of Energy. Ames Laboratory is operated for the U. S. Department of Energy by Iowa State University under Contract No. DE-AC02-07CH11358. Use of the Advanced Photon Source was supported by the U. S. DOE under Contract No. DE-AC02-06CH11357.

-
- ¹ L. Fu and C. L. Kane, Phys. Rev. B **76**, 045302 (2007).
 - ² D. Hsieh, D. Qian, L. Wray, Y. Xia, Y. S. Hor, R. J. Cava, and M. Z. Hasan, Nature **452**, 970 (2008).
 - ³ Y. Xia, D. Qian, D. Hsieh, L. Wray, A. Pal, H. Lin, A. Bansil, D. Grauer, Y. S. Hor, R. J. Cava, et al., Nat. Phys. **5**, 398 (2009).
 - ⁴ H. Zhang, C. X. Liu, C. L. Qi, X. Dai, Z. Fang, and S. C. Zhang, Nat. Phys. **5**, 438 (2009).
 - ⁵ Y. L. Chen, J. G. Analytis, J.-H. Chu, Z. K. Liu, S.-K. Mo, X. L. Qi, H. J. Zhang, D. H. Lu, X. Dai, Z. Fang, et al., Science **325**, 178 (2009).
 - ⁶ M. Z. Hasan and C. L. Kane, Rev. Mod. Phys. **82**, 3045 (2010).
 - ⁷ J. E. Moore, Nature **464**, 194 (2010).
 - ⁸ R. Li, J. Wang, X.-L. Qi, and S.-C. Zhang, Nat. Phys. **6**, 284 (2010).
 - ⁹ P. Hosur, S. Ryu, and A. Vishwanath, Phys. Rev. B **81**, 045120 (2010).
 - ¹⁰ R. S. K. Mong, A. M. Essin, and J. E. Moore, Phys. Rev. B **81**, 245209 (2010).
 - ¹¹ S. Chadov, X. Qi, J. Kübler, G. H. Fecher, C. Felser, and S. C. Zhang, Nat. Mat. **9**, 541 (2010).
 - ¹² H. Lin, L. A. Wray, Y. Xia, S. Xu, S. Jia, R. J. Cava, A. Bansil, and M. Z. Hasan, Nat. Mat. **9**, 546 (2010).
 - ¹³ D. Xiao, Y. Yao, W. Feng, J. Wen, W. Zhu, X.-Q. Chen, G. M. Stocks, and Z. Zhang, Phys. Rev. Lett. **105**, 096404 (2010).
 - ¹⁴ C. Li, J. S. Lian, and Q. Jiang, Phys. Rev. B **83**, 235125 (2011).
 - ¹⁵ T. Graf, S. S. P. Parkin, and C. Felser, IEEE Trans. Magn. **47**, 367 (2011).
 - ¹⁶ P. C. Canfield, J. D. Thompson, W. P. Beyermann, A. Lacerda, M. F. Hundley, E. Peterson, Z. Fisk, and H. R. Ott, J. Appl. Phys. **70**, 5800 (1991).
 - ¹⁷ G. Goll, M. Marz, A. Hamann, T. Tomanic, K. Grube, T. Yoshino, and T. Takabatake, Physica B **403**, 1065 (2008).
 - ¹⁸ N. P. Butch, P. Syers, K. Kirshenbaum, A. P. Hope, and J. Paglione, arXiv:1109.0979 (2011), unpublished.
 - ¹⁹ Z. Fisk, P. C. Canfield, W. P. Beyermann, J. D. Thompson, M. F. Hundley, H. R. Ott, E. Felder, M. B. Maple, M. A. L. de la Torre, P. Visani, et al., Phys. Rev. Lett. **67**, 3310 (1991).
 - ²⁰ P. Wosnitza, G. Goll, A. D. Bianchi, B. Bergk, N. Kozlova, I. Opahle, S. Elgazzar, M. Richter, O. Stockert, H. v. Löhneysen, et al., New J. Phys. **8**, 174 (2006).
 - ²¹ A. E. Dwight, in *Proceedings of the 11th Rare Earth Research Conference*, edited by J. M. Haschke and H. A. Eick (U. S. Atomic Energy Commission, 1974), vol. 2, p. 642.
 - ²² R. A. Robinson, A. Purwanto, M. Kohgi, P. C. Canfield, T. Kamiyama, T. Ishigaki, J. W. Lynn, R. Erwin, E. Peterson, and R. Movshovich, Phys. Rev. B **50**, 9595 (1994).
 - ²³ R. H. Forster, G. B. Johnston, and D. A. Wheeler, J. Phys. Chem. Solids **29**, 855 (1968).
 - ²⁴ P. C. Canfield and Z. Fisk, Phil. Mag. B **65**, 1117 (1992).
 - ²⁵ J. W. Kim, Y. Lee, D. Wermeille, B. Sieve, L. Tan, S. L. Bud'ko, S. Law, P. C. Canfield, B. N. Harmon, and A. I. Goldman, Phys. Rev. B **72**, 064403 (2005).
 - ²⁶ M. E. Fisher, Phil. Mag. **82**, 1731 (1962).
 - ²⁷ C. Detlefs, A. H. M. Z. Islam, A. I. Goldman, C. Stassis, P. C. Canfield, J. P. Hill, and D. Gibbs, Phys. Rev. B **55**, R680 (1997).
 - ²⁸ H. You, J. Appl. Cryst. **32**, 614 (1999).
 - ²⁹ J. W. Kim, A. Kreyssig, L. Tan, D. Wermeille, S. L. Bud'ko, P. C. Canfield, and A. I. Goldman, Appl. Phys. Lett. **87**, 202505 (2005).
 - ³⁰ G. Goll, O. Stockert, M. Prager, T. Yoshino, and T. Takabatake, J. Mag. Magn. Mat. **310**, 1773 (2007).
 - ³¹ C. Liu, Y. Lee, T. Kondo, E. D. Mun, M. Caudle, B. N. Harmon, S. L. Bud'ko, P. C. Canfield, and A. Kaminski, Phys. Rev. B **83**, 205133 (2011).